Pulse Shape-Induced Global Phase Crosstalk in Heterodyne DAS

Thomas Lauber, Francesca Celine Catalan, Kevin Wilma, Gregor Cedilnik, Gareth Lees

AP Sensing GmbH, Herrenberger Straße 130, 71034 Böblingen, Germany

info@apsensing.com

Abstract: The performance of a distributed acoustic sensor (DAS) depends on the spectral properties of the probe light used. This involves the coherence properties of the light source as well as the envelope of the emitted pulses. Here, we discuss phase errors and crosstalk that arise from pulse shape side lobes exceeding the heterodyne frequency shift.

Introduction Distributed acoustic sensing (DAS) has become an important approach to vibration measurements in various applications, such as pipeline and energy cable monitoring, structural integrity monitoring, and seismic surveys in oil and gas fields. Owing to its high sensitivity, fast detection response, and distributed nature, DAS provides real-time quantitative visualization of acoustic events over long distances with high spatial resolution [1].

The general principle behind this technology is rooted in the high sensitivity of the optical phase to acoustic signals in the vicinity of a sensing fiber. These perturbations manifest in the DAS signal as a distributed speckle pattern variation resulting from the coherent interference of the Rayleigh backscatter from multiple scattering centers within the probed fiber range [2]. In the heterodyne DAS scheme, this backscatter signal is combined with an optical local oscillator of a different frequency to form a beat signal as it reaches the detector. Ideally, the phase change by the acoustic event can be directly extracted by demodulating the signal from the heterodyne carrier. However, the speckle nature of the signal also means that quasi-random phase variations and destructive interference ('fading') can occur, which may contribute to errors in the phase extraction. Any global phase change at a position before the probed fiber range arising from temperature drift or acoustic events may affect these faded spots differently, manifesting as global phase crosstalk between different parts of the fiber.

In this work, we elucidate the mechanism behind this global phase crosstalk in heterodyne DAS. We numerically and experimentally demonstrate that pulse apodization helps to mitigate this effect. While it is desirable to have steep pulse edges for optimum spatial resolution and minimum chirp distortion through self-phase modulation, the performance may suffer when the pulse envelope spectrum has significant side lobes [3]. Indeed, previous works have shown that compared to the typically-used rectangular pulses, smoothed pulses minimize the spectral side lobes, resulting in improved signal-to-noise ratio [4] and reduced fading due to modulation instability [5]. Here, we confirm the positive effects of using smoothed pulses in minimizing the global phase crosstalk.

Modeling In a heterodyne DAS the electric field of the local oscillator E_{LO} interferes with the backscatter E_{BS} which results in a total field E_{Det}. On detection this is converted into a photocurrent S_{Det} proportional to optical power:

$$E_{Det} = E_{BS} + E_{LO} \quad \text{with} \quad E_{BS}(t) = \int A(\omega_0 + \Delta\omega) e^{-i(\omega_0+\Delta\omega)(t+\Delta t)} d\Delta\omega \quad \text{and} \quad E_{LO}(t) = A_{LO} e^{-i\omega_0 t} \tag{1}$$

$$S_{Det} = E_{Det} E_{Det}^* = E_{BS}E_{BS}^* + E_{BS}E_{LO}^* + E_{BS}^* E_{LO} + E_{LO}E_{LO}^* \quad . \tag{2}$$

Where t corresponds to the time-of-flight of the light from pulse emission to detection, while Δt represents an additional, potentially variable, time delay on the probe light before the location of interest. The time delay may be caused by the instrument (like component phase noise), or by changing fiber properties (i.e. strain or temperature). The amplitude spectrum $A(\omega_0 + \Delta\omega)$ mainly depends on the pulse shape of the light in the time domain.

The constant terms ($E_{BS}E_{BS}^*$ and $E_{LO}E_{LO}^*$) can be ignored when extracting the phase, and they are usually removed by balanced detectors, while the oscillating terms $E_{BS}E_{LO}^*$ and $E_{BS}^* E_{LO}$ are measured. We replaced Δt by the corresponding phase shift at the local oscillator frequency ω_0 by using the relation $\phi = \Delta t\, \omega_0$ to represent the global phase variation in front of the location of interest. This, combined with the approximation $\frac{\Delta\omega}{\omega_0}\phi \approx 0$, simplifies the oscillating terms. The first term reduces to

$$E_{BS}(t) E_{LO}^*(t) = A_{LO}^* e^{-i\phi} \int A(\omega_0 + \Delta\omega) e^{-i\Delta\omega t} d\Delta\omega \tag{3}$$

and analogously, the complex conjugate can be calculated for the second oscillating term $E^*_{BS}E_{LO}$.

Phase extraction methods essentially calculate the relative phase of the signal to a reference. Due to its computational efficiency, we decided to extract the phase by digital down conversion - i.e. digitally mixing the signal with an artificial reference ($e^{-i\omega_h t}$) and applying a low-pass filter lp (with a cut-off frequency ω_{cut}).

$$S_{Det,AC}(t)e^{-i\omega_h t} = A^*_{LO}e^{-i\phi}\int A(\omega_0+\Delta\omega)e^{-i(\Delta\omega+\omega_h)t}d\Delta\omega + A_{LO}e^{i\phi}\int A^*(\omega_0+\Delta\omega)e^{i(\Delta\omega-\omega_h)t}d\Delta\omega \quad (4)$$

$$\Rightarrow z := lp(S_{Det,AC}(t)e^{-i\omega_h t},\omega_{cut}) \rightarrow \phi_{meas} = \mathrm{atan2}\,(Im(z),Re(z)) \quad (5)$$

Where z represents the complex phasor of the signal containing the amplitude and phase. The derived acoustic signal at a certain location is obtained by pairwise differencing the phase results of locations separated by the gauge length g_L: $\Delta\phi_{g_L} = \phi(x+\frac{g_L}{2}) - \phi(x-\frac{g_L}{2})$. Both oscillatory terms within the integrals in equation 4 contribute after low-pass filtering, one for $\Delta\omega \approx +\omega_h \pm \omega_{cut}$ and the other for $\Delta\omega \approx -\omega_h \pm \omega_{cut}$. This implies that the system gives an output for both positive and negative frequency shift of the backscatter with respect to ω_0 and thus cannot distinguish between the two signals and instead outputs a superposition. This is inherent to a heterodyne architecture as the detector is only able to detect the power of the signal. Note that in equation 4 the integrals evaluate to a complex value depending on t which means that they depend on time-of-flight and thus position, while the prefactors $e^{\pm i\phi}$ depend on the global phase but react with the opposite sign on changes of ϕ.

As the integrals in equation 4 require numerical treatment, we illustrate the main consequences of this with a simplified backscatter spectrum $A_m = A\delta(\omega_h) + rA\delta(-\omega_h)$ composed only of the heterodyne frequency and the frequency mirrored at ω_0. r is the amplitude ratio of the two frequency components. With this approximation, the integrals in the equation can be evaluated directly. Applying this to equation 4 and removing terms with frequencies above ω_{cut} (due to the low-pass results) in

$$z := lp(S_{Det,AC,m}(t)e^{-i\omega_h t},\omega_{cut}) = A_{LO}A\left[e^{-i\phi}r + e^{i\phi}\right] \quad \Rightarrow \quad \phi_{meas} = \mathrm{atan}\left(\frac{1-r}{1+r}\tan\phi\right) \quad (6)$$

Where $\mathrm{atan2}(x,y)$ is replaced with $\mathrm{atan}(x/y)$, valid for $-\pi/2 < \phi < \pi/2$. This results in the simple relation for the measured phase ϕ_{meas}. As one can see from this result, the measured phase is identical to the true phase for $r = 0$. With increasing r, which means that the negative frequency component relatively increases in amplitude, the relation becomes increasingly nonlinear until a flip in sign appears at $r > 1$. Effectively, for $r > 1$, the negative frequency component is stronger than the original frequency. This variation in the ratio can occur in case fading of the two components happens. Figure 1(a) shows a few examples of phase error curves $\phi_{err} = \phi_{meas} - \phi$ for different r as a function of the true global phase.

Numerically evaluating equations 4 and 5 generates analogous error curves. In Figure 1(b)-(d) this is displayed for three sample pulse shapes: a rectangular pulse, a Tukey window with $\alpha = 0.5$, and a Blackman window (note the differing vertical axis). For each pulse shape the parameters are chosen to provide the same full width at half maximum (FWHM). Therefore, they all have a similar width of the main lobe, but - from left to right - significantly decreasing amplitude of the side lobes.

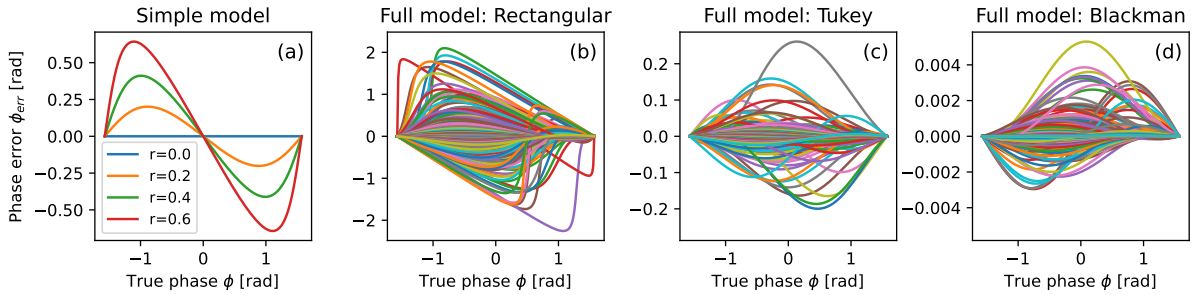

Fig. 1. (a) Phase error results of the simple model in equation 6 for different ratios r of the negative to positive frequency components. (b)-(d) Random selection of phase error curves by integrating the full model in equations 4 and 5 evaluated for different pulse shapes. Note the different vertical axes among the plots.

As the integrals in equation 4 depend on time-of-flight t they evaluate differently at different locations. In Figure 1(b)-(d), the different curves, which correspond to a random selection of locations, show the variability of not only the amplitude, but also the shape of the curves. Additionally, the properties of the fiber (like the random distribution of the scatter centers) can change the phase distribution of $A(\omega)$ and affect the integral result.

In Figure 1(a), the peak amplitudes of the error curves are directly related to the ratio r, while in Figure 1(b)-(d) the ratio implicitly follows from the amplitude ratios of the side lobes at the negative heterodyne shift to the main lobe. This results in a significant reduction of the errors when using smoother pulses.

The curves in Figure 1 are periodic and a variation in the true phase that is linear over time will result in an oscillation of the measured phase. Even if gauge length differencing is applied, it cannot be assumed that both locations have the same error curve, and thus a global phase change does not necessarily cancel out as expected.

As the error curves have a period of π, the apparent base frequency of the errors will be twice the change rate of the global phase. Also, the light passes a disturbed section twice, the global phase change-related frequency from a single acoustic event is expected to be doubled. In total, we expect the artifacts to exhibit 4 times the frequency of the phase slope of the source of the disturbance. Also, due to the nonlinearity, harmonics are likely to appear.

A global phase that varies with a large magnitude experiences aliasing and is wrapped quasi-randomly around the full 2π range. This will manifest in the DAS signal as an increased noise floor. This happens, in particular, for long distances where several disturbances accumulate.

In consequence artifacts due to events can appear at similar or harmonic frequencies at random positions after the event itself and the appearance of the artifact can be modified by additional events like temperature variations.

Experimental verification We constructed an experimental setup to demonstrate the modeled artifacts and the effectiveness of shaping the pulse to reduce them. The heterodyne DAS configuration utilized in this work can be broken down into three main parts: (1) pulse generation and amplification, (2) heterodyne carrier modulation and pulse shaping, and (3) detection (Figure 2). Continuous-wave laser light is generated via a narrow linewidth diode laser at 1550 nm and shaped to create pulses with a duration of 50 ns and pulse repetition frequency of 10 kHz. The peak power is amplified and controlled by an erbium-doped fiber amplifier (EDFA). Both the frequency shift and pulse shaping are performed by an acousto-optical modulator (AOM) controlled by an arbitrary waveform generator (AWG). The properties of the AWG-generated waveform, the pulse duration, and the EDFA pump current were judiciously chosen either to maintain the rectangular pulse from the pulser or provide apodization into a smoothed pulse, using a Tukey window with a large α, with the same 50-ns FWHM and equivalent pulse energy. To reduce any side effects arising from disturbances of the fiber under test (FUT), we placed the FUT in a vibration-isolated and temperature-stabilized environment.

We introduced a distinct frequency artifact by detuning the clock of the driving frequency of the AOM, which results in a continuous linear phase drift corresponding to a frequency of $f_{drift} = 360\,\mathrm{Hz}$. We then monitored how this artifact responds to a controlled global phase variation due to a physical change in the optical fiber path in front of the analyzed fiber section via a piezo electric fiber stretcher.

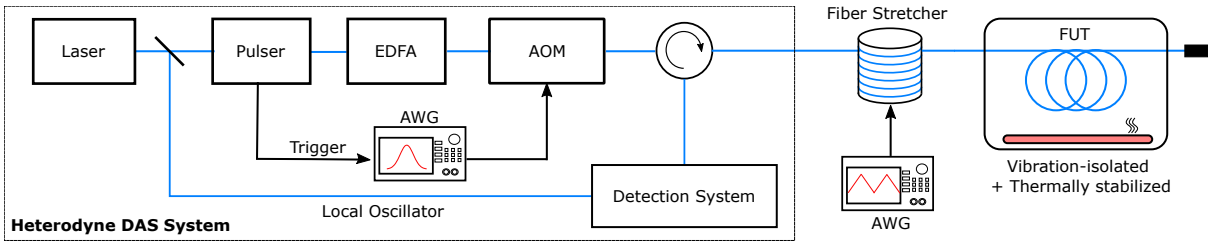

Fig. 2. Architecture and experiment overview.

Figure 3 shows the results of measurements taken 300 m after the fiber stretcher location. The first row shows the corresponding mean spectrum averaged over the whole duration of the lower plots (20 s). The four spectrograms in (c) - (f) were calculated by spatially averaging the spectra over a distance of 500 m. The shape of the respective pulses generated by the AOM are shown in the insets. The continuous phase drift of the AOM alone results in a frequency peak at $2 \cdot f_{drift} \approx (723 \pm 10)\,\mathrm{Hz}$, as shown in the blue curve in the first row and the spectrograms in the second row. The slight variations of the frequency are attributed to residual temperature variations. The frequency peak matches $2 \cdot f_{drift}$ closely as the frequency is doubled due to the period of the error curves (see Figure 1). While the artifact does not shift in frequency no matter which pulse shape is used, its peak amplitude is decreased by as much as 6 dB when smoothed pulses are employed (Figure 3 (b)). As predicted by the model, the minimized sidelobes of the Tukey window-apodized pulse led to a reduced global phase crosstalk.

The effect of driving the fiber stretcher with a triangular voltage ramp with a low gradient can be observed in the orange curves in Figure 3 (a) and (b) and in the spectrograms in Figure 3 (e) and (f). The original peak is shifted to higher frequencies during ramp-up of the stretcher and to lower frequencies during ramp-down, resulting in the alternating pattern. We can quantify the frequency shifts as follows. The linear phase ramps have a peak-

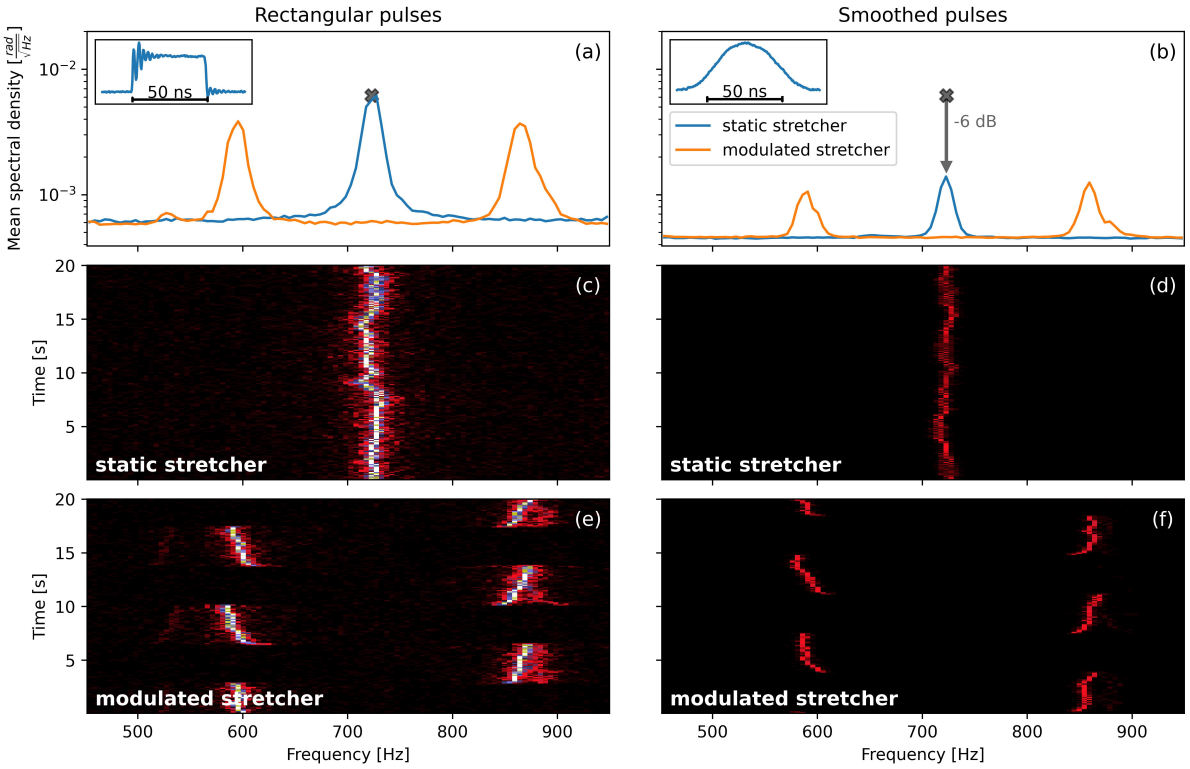

Fig. 3. Phase crosstalk observations. (a) - (b) Line plots and (c) - (f) spectrograms of recorded signals averaged over 500 m (gauge length = 10 m, color scales aligned). The left column (a), (c), (e) and right column (b), (d), (e) correspond to rectangular and smoothed pulses, respectively. The insets in (a) and (b) show the measured pulse shape (ringing originates from the detector).

to-peak amplitude of 805 rad for uni-directional transmission with a period of 7.3 s. This results in linear global phase ramps with a gradient of ± 220.6 rad/s. The gradient must be doubled due to the period of the error curves, while another factor of 2 comes from the light passing the stretcher twice before detection. Thus, the expected frequency shift is $\Delta f_{shift} = 140$ Hz. On the other hand, a mean shift of $\Delta f_{split,meas} \approx (135 \pm 8)$ Hz is extracted from the experiments, which matches the expected within the measurement accuracy.

As before, smoothing the probe pulses reduces the amplitude of the frequency-shifted artifact by 6 dB.

Conclusion In this paper we have modeled and experimentally demonstrated that, in heterodyne DAS systems, careful design of the pulse shape is essential to avoid crosstalk between the global phase and the derived acoustic signal. The global phase was shown to be altered by acoustic events in front of the location of interest and phase variations in the DAS system, manifesting as an artifact on the DAS signal at locations of unaltered fiber behind the source of the phase variations. In the case of random global phase, an elevated broadband noise floor is expected, which adds to other noise sources. Smoothing the pulse envelope can reduce these artifacts significantly by at least a factor of 4, as shown in the experiments. The presented discussion aims to provide guidance and enable improvements of the design and signal quality of heterodyne DAS systems.

References

1. G. Cedilnik, G. Lees, P. E. Schmidt, S. Herstrøm, and T. Geisler, "Pushing the reach of fiber distributed acoustic sensing to 125 km without the use of amplification," IEEE Sensors Lett. **3**, 1–4 (2019).
2. P. Lu, N. Lalam, M. Badar, B. Liu, B. T. Chorpening, M. P. Buric, and P. R. Ohodnicki, "Distributed optical fiber sensing: Review and perspective," Appl. Phys. Rev. **6**, 041302 (2019).
3. J. J. Mompó, S. Martín-López, M. González-Herráez, and A. Loayssa, "Sidelobe apodization in optical pulse compression reflectometry for fiber optic distributed acoustic sensing," Opt. letters **43**, 1499–1502 (2018).
4. F. Uyar, A. Nehir, T. Kartaloğlu, E. Özbay, and I. Özdür, "The pulse shape effect on signal-to-noise ratio for ϕ-otdr systems," in *Optics InfoBase Conference Papers,* (The Optical Society, 2021).
5. M. R. Fernández-Ruiz, H. F. Martins, J. Pastor-Graells, S. Martin-Lopez, and M. Gonzalez-Herraez, "Phase-sensitive otdr probe pulse shapes robust against modulation-instability fading," Opt. Lett. **41**, 5756–5759 (2016).